VFAST Transactions on Mathematics
http://vfast.org/journals/index.php/VTM@ 2025 ISSN(e): 2309-0022, ISSN(p): 2411-6343
Volume 13, Number 2, July-December, 2025 *pp: 20-40*

Establishing Neural Network Models for Predicting Flood Propagation and Recession in Urban Roads

Muhammad Fawad Khan [1], **Fazl Ullah Fazal** [2], **Awais Khan** [3*], **Muhammad Saad** [2]

[1]School of Information Technology and Systems, University of Canberra, Bruce 2617, ACT, Australia; [2]Department of Mathematics, Abdul Wali Khan University Mardan, Pakistan; [3]Victorious College Yar Hussain, Swabi, Khyber Pakhtunkhwa, Pakistan 23320

Keywords: *Machine learning, Flood propagation, Road networks, Artificial neural network, RK4 technique, Surrogate model, Levenberg–Marquardt method, soft computing.*

Journal Info:
Submitted:
March 28, 2025
Accepted:
December 17, 2025
Published:
December 31, 2025

Abstract

In this analysis, a contagion model is a straightforward yet effective mathematical approach—that was used to forecast the temporal change of the outset and contiguous distribution and recession of flooding in metropolitan roadway networks. A system of metropolitan roadways must be flood-resistant in order to provide public services and deal with emergencies. The dispersion of floodwaters is a complicated temporal-spatial process that affects urban networks. In comparison to the SEIR (Susceptible-Exposed-Infected-Recovered) prototype, a system of ordinary differential equations, four macroscopic characteristics, rate of including flood spreading represented by (β), rate of flood incubation symbolized by (α), and rate of recovery highlighted by (μ), can be used to understand how floods evolve within networks. Additionally, by joining the backpropagated neural network and the Levenberg—Marquardt algorithm (NN-BLMA), surrogate solutions to the model are discovered. This method has some clear advantages over conventional ones, including flexibility, comparatively simple implementation, and fastest results. Reference solutions are generated using the Runge-Kutta of order four (RK4) method. We have examined three distinct scenarios to analyze our surrogate solution models. By changing α, β, μ, and k, the mathematical model's stability and equilibrium are examined. To gauge the validity of our machine learning process, we categorize our candidate solutions into training, testing, and experimental class. The efficacy of the NN-BLMA scheme has been confirmed by comparative examinations of statistical values based on mean squared error function (MSEF), effectiveness, regression plots, and failure histograms.

***Correspondence Author Email Address:**
mawaiskhan778@gmail.com
DOI: 10.21015/vtm.v13i2.2106

1 Introduction

In light of the crucial part that transportation plays in the handling of emergency situations, the delivery of necessary services, and the upkeep of economic prosperity [1], the resistance of metropolitan road networks to natural threats, rising amount of attention, especially particular incidents of floods [2, 3]. Metropolitan networks are subject to floods that spread across space and time, and a significant amount of spatial-temporal ambiguity is created, which has an impact on preventative measures like evacuation and swift emergency response [4]. The improvement of urban road network resilience depends on the development of efficient prediction technologies to foresee the features of flooding episodes [5]. Much research has been conducted to investigate the spatial and temporal features of floods in urban networks. These studies looked at the effects of stressful circumstances [6–8] as well as cascading impact on roads system [9, 10]. Empirical research using satellite photos remote sensors [11], hydraulic data [12], or remote sensors [11], in particular, have tried to capture the features of urban flooding. The profile of stressful environments over time, like the length of time that cyclones continue to produce rainfall, is one of the primary drivers of the temporal evolution of flood status [12]. This temporal information makes it easier to identify the outbreak as well as the points of inflection for floods in networks that have been affected. Flooding also shows a high degree of spatial correlation [13], which means that road segments that are co-located with one another have a greater chance of being flooded in the time increments that immediately follow them, as shown by the model's digital timestamps [14]. For instance, a hydrologic analysis of regional flooding quantiles for 575 Austrian catchments revealed that the regional frequency of floods can be accurately predicted by one's closeness to flooded areas. This information was found through the application of justified flood quantiles [15]. Although empirical investigations have shown the intricate temporal-spatial dynamics of floods, their ability to forecast floods frequently depends on various hydro-geomorphological inspecting datasets and rigorous calculation [16]. Because they take too long and cost too much to run, the current physics-dependent hydrodynamic paradigms may not be capable of producing accurate predictions about flood propagation and road segment downfall in a very short time frame [17].To address the shortcomings of numerical approaches, machine learning algorithms have been created and evaluated in the context of forecasting the movement of floods in metropolitan settings [18, 19].

Without dependence on a variety of source variables and historical information, like the amount of water and the breadth of the roadways, a mathematical formulation that can depict the temporal-spatial course of floods is needed is actually necessary given the flaws of existing models. Recent research has shown that spreading happens in a range of systems, such as the development of transportation traffic jams, the spread of transmissible diseases among people, the dispersal of ideas in social networks [20], and the development of inundation in metropolitan networks of road [21, 22], share a surprising degree of similarity with one another. Our study intended to characterize the flood's spreading mechanism using generalized mathematical transmission paradigms, such as conventional epidemic prediction models. These studies served as the basis for this research [23]. The currently available models of epidemics provide a numerical and analytical framework to measure and forecast numerous propagating events in a range of different scenarios. The well-known susceptible-infectious-recovered (SIR) prototype, in particular, was responsible for the creation of the fundamental components of epidemic modeling through the utilization of infectious and recovery rates. Two key ideas underlie these mathematical models: homogeneous mixing, where each entity has an equal chance of coming into contact with an infected entity,

and compartmentalization, where each entity is linked with a chamber [24]. Each road cell has a corresponding flood status when there is flooding, either functional flow or flooded. That's why I think the compartmentalization concept works for the flooding propagation problem. The modeling of contagion is greatly simplified by these theories since mathematical simulation can still show time development. of the proportion of affected individuals in the networks without requiring knowledge of the network's geometry.

The task of predicting flood risk should consider the floodwater's temporal and spatial characteristics in roadway networks. In addition to determining the percentage of roads under flood at each timestamp, metropolitan flood threat characterization requires pinpointing the locations of flooded roads as flooding happens. Thus, these requirements cannot be met by pure mathematical models. The network percolation procedure has lately received attention in this area because it can encapsulate the spreading mechanism via topological connectivity in networks [25]. According to percolation theory, the likelihood of infected neighbors spreading an illness depends on the assumption that local network components exhibit heterogeneous mixing [26]. The edges of the percolated network are particularly where the infection progresses from a starting node [27]. As a result, the percolation process weakens contacts over the entire network and represents the "amplification" impact of neighbors. The likelihood of an illness spreading to anyone the node comes into contact with is higher. Given that it takes into account the geographical restrictions and co-location of urban networks, this characteristic is crucial for the prediction of flood propagation in metropolitan networks. The percolation mechanism would not be able to show the temporal progression of floods in metropolitan networks without the time data on the fraction of flooded roadways.

The implementation of optimization techniques for solving nonlinear differential equations has recently been the subject of research. To enhance a specific procedure while staying within the constraints of an assignment or program, we refer to optimization as the application of standardized operations, strategies, subject areas, and tactics. There are a variety of approaches one can take in order to modify a process in such a manner that it functions more efficiently than it did in the past. This can be accomplished through. Deleting a process step, creating a new process step, or revising an existing process phase are examples of simplifications that can aid in the streamlining of a workflow. Recent times have seen the application of optimization methods for the purpose of optimizing the weights in neural networks. Recent times have seen the application of optimization methods for the purpose of neural network weight optimization. The initial studies that would eventually become the area of neural network science were conducted in the early twentieth and late nineteenth centuries (ANNs). The primary emphasis of this research was placed on collaborative efforts among researchers in the domains of neurophysiology, physics, and psychology. Even though this early research concentrated on basic concepts related to perception, conditioning, and learning, among other subjects, It failed to offer precise mathematical models of the behavior of neurons in particular networks. As a consequence of these most recent developments, the investigation of neural networks has been given a second chance at life. Academics have studied a huge spectrum of ANN types during the last two decades, publishing a considerable number of research papers in the process. The most widely used artificial neural networks (ANNs) for a variety of problems are those that use supervised learning and have three layers: an output layer, a hidden layer, and an input layer. Figure (1) these are the kind of ANNs that are called artificial neural networks (ANNs).

Several applications of neural networks have recently been utilized in conjunction with optimization techniques to handle a wide range of problems. The ODE system's solution for flood retraction and spread in urban metropolitan roadway networks, as well as a prototype of flood spreading and retrac-

tion in metropolitan roadway networks, are examples of these issues involving the use of a neural network with a feed-forward architecture to propagate floods. Because of the significance of this research, we have been inspired to implement and enhance the performance of the ODE system and the solutions, further developing the idea of supervised machine learning. The following is a list of important aspects that will be covered in the planned research:

- A revolutionary approach to machine learning is carried out in the targeted system by a computer that is not impacted or subject to the singularity and continuity of the ODE.
- Multidimensional data can be applied with methods of machine learning. By using the Levenberg-Marquardt method for local search optimization, they may efficiently supervise the provided data.
- The method's consistency and effectiveness are shown by the procedure's smooth convergence throughout the optimization of an optimization problem determined by the measure of mean square error.

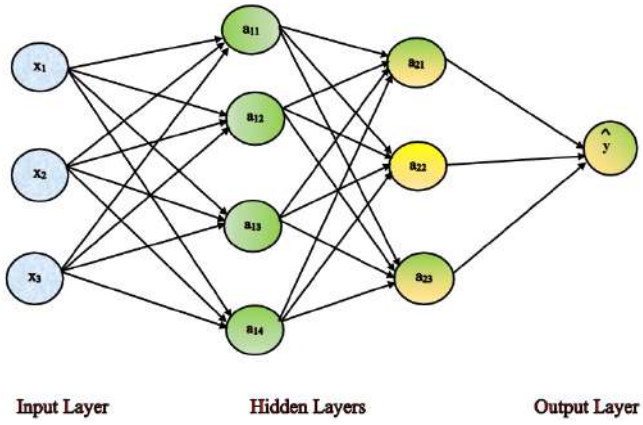

Figure 1. Three-layer feed-forward neural network's architecture.

2 Flood Propagation Model and Road Networks

The model that is being presented includes the following components: modeling of road networks, characterization of flood spread, and model solution utilizing artificial neural networks (ANN). This paradigm of flooding propagation in metropolitan road networks is similar to that of an epidemic. It takes into account both the regional possibility of flooding influencing other nearby roads as well as the overall dynamics of flood levels.

2.1 Modeling of the Road Network

There is an emphatically large number of road sections in a network, with the majority being between 100 and 800 meters each. The information on the state of the traffic that is collected at the level of the road segment offers adequate spatial resolution to properly evaluate the extent to which road networks are impacted by flooding.

In order to facilitate the process of locating a point on a geographical map, each point has a longitude and a latitude assigned to it. As a result, a road section may be demonstrated as (lng_s, lat_e, lat_s, lng_e), here the starting mark's longitude lng_s and latitude lat_s and the ending mark's longitude lng_e and latitude lat_e. Banded road segments often do not enclose flooded areas, despite the fact that they offer a useful resolution for understanding the situation in metropolitan networks. This is despite the fact that road segments offer a better knowledge of the situation. In addition, the vast segments and the intricate linkages between them in the networks would result in a substantial increase in the amount of processing that was required. As a result, when it comes to modeling road networks, segment-to-segment modeling must be restricted to ensure efficient calculation and to follow the natural pattern of flood spread. In order to accomplish this goal, grid decomposition, a method that is quite common, was utilized in this study to generate cells of identical size and to partition the overall study area into several smaller sections.

The geo-coordinates (lng_{bl}, lat_{bl}, lng_{ur} lat_{ur}) of the cell's spatial boundary can be used to describe it. lng_{bl} and lat_{bl} are the longitude and latitude of the bottom left corner, while lng_{ur} and lat_{ur} are the longitude and latitude of the upper right corner. We use the following standards on the road network to convert the road segments to the grid:

$$s_i \in grid_j, if lat_{bl} \leq \frac{lat_s + lat_e}{2} \leq lat_{ur} and lng_{bl} \leq \frac{lng_e + lng_s}{2} \leq lng_{ur}. \quad (1)$$

Once a grid decomposition has been performed, one way to conceptualize the road network that is assembled from individual roadway sections is as a collection of cells.

In actuality, how the grid was decomposed would be determined by a variety of different factors. For example, a large cell would be composed of multiple segments, which could lead to a reduction in the spatial resolution of the image. As a consequence of this, The model's capacity to depict the spatial spread of the flood would be further hampered. A narrow grid that cannot encompass at least one road section, on the other hand, will fragment the network into discontinuous components, which will lead to an increase in the computing cost. As a result, grid decomposition calls for preliminary testing to guarantee that each cell in the grid can keep its spatial resolution without unreasonably taxing the computational resources of the system. To cut down on the amount of computing work required, once the road segments have been assigned to cells, cells that are empty will be removed. The remaining cells come together to form a network, with the cells themselves serving as nodes in the network, and the common borderlines between the cells serving as links. If we follow these steps, With an average degree of k, we will be able to create an erratic grid network G that closely resembles the structure of the road networks. The number of cells typically found next to a given cell in the road system is referred to as the cell's average degree.

Next, a dynamical binary phase parameter called x are being associated with each one of the grid network G's N cells (also known as nodes), so that the quantity of the variable $xi(t)$, which ranges from 0 to 1, indicates the flood position of node i at the moment t. We use conventional terminology to categorize the cells as either "functional flow" (F) or "flooded" (C), with F and C corresponding to x = 0 and 1, respectively. When a road is in functional flow, traffic can use it (regardless of traffic level). The flooded cells are represented by state C within the scope of the flooding propagation procedure. The portion of flooded cells c(t) = $\frac{1}{N} \sum_{i=1}^{n} x_{i(t)}$ determines the macroscopic flooding event t.

3 Characterization of flood spread

In terms of time and location, flood spreading and recession mechanisms vary. The model under consideration takes into account macro-characteristics to anticipate the temporal dynamics of deluge dispersion in metropolitan networks and in metropolitan roadway networks to depict the time dimension of flood progression, see Figure (2). We construct four flooding states for a cell in the first stage by incorporating the temporal attributes: exposed, functional flow, recovered, and flooded. At time t, C(t) indicates the amount of flooded units in the network; The quantity of functional downstream cells at time t is represented by F(t); R(t) reflects the proportion of units that recovered successfully from flooding at time t, whereas E(t) is a representation of how many cells (i.e., roadways that are in the path of incoming floodwater but where traffic is still flowing) are still in the floodwater incubation phase. Every cell in the grid network G at time t = 0 exhibits functional flow with a total of N nodes and an average degree of k. It follows that C(t = 0) = 0 and F(t = 0) = N. Starting at a specific group of nodes, the flood spreads laterally throughout the network. A unit in the undirected network is often linked to k other units from a macroscopic standpoint. A cell that has flooded exposes its neighbors to flooding at a rate of *beta*. It is believed that the connections between the cells are homogenous for modeling temporal evolution, which serves as the foundation for creating a system of generic differential equations. The likelihood that a functional flow connection is linked to a flooded unit at time t is then given by F(t)/N. kF(t)/N therefore interacts with a flooded cell. Water flows through each cell in the C(t) flooded cells at a rate of *beta*, and exposed cells turn into flooding at a constant rate *alpha*, The average amount of newly uncovered cells, dE(t), over a unit time interval, dt is calculated using the formula below:

$$\frac{dE(t)}{dt} = \frac{(N - R(t) - E(t) - C(t))C(t)}{N}\beta k - \alpha E(t). \tag{2}$$

Traffic can still move through the exposed cells, which aren't submerged yet, but they might be flooded in the next time frames. This phase is known as the flood incubation phase. A road cell can only be in one of the four defined states of the roadway units. Hence, N should be the result of adding the four status elements. That is; E(t) + R(t) + F(t) + C(t) = N. For expressing the portion of units in each status, we use the following parameters: c(t) represents the portion of grid cells that are flooded at time t; The portion of functional-flow units having accessible road segments at time t is expressed by the symbol f(t); The portion of cells that recovered from flooding during period t is expressed by r(t); and The portion of cells that faced exposure to flooding at time t but are still in flood incubation is indicated by the symbol e(t). Therefore below are the ODE calculations for the rate of change of exposed units.

$$\frac{de(t)}{dt} = (1 - c(t) - r(t) - e(t))k\beta c(t) - e(t)\alpha. \tag{3}$$

The product of *beta* k is known as the rate of transmission or transmissibility. The transmissibility of floodwater can be used to assess its potential to dispersion across a metropolitan network at the same spreading rate. This helps us to comprehend the consequences of the topological framework of a metropolitan network on floodwater transmission. Every timestamp causes a section of the functional-flow units to become naked, hence the following expression can be used to indicate the rate at which this portion is reducing:

$$\frac{df(t)}{dt} = -\beta(1 - r(t) - e(t) - c(t))c(t)k. \tag{4}$$

A portion of the exposed nodes could flood concurrently at a α rate in a unit time frame. Moreover, certain of the flooded units are being restored at a cost of μ. As a result, the following formula can be used to express the rate of change of the proportion of flooded units and the proportion of recovered cells:

$$\frac{dc(t)}{dt} = e(t)\alpha - c(t)\mu. \tag{5}$$

$$\frac{dr(t)}{dt} = c(t)\mu. \tag{6}$$

The likelihood of a flooded unit being linked to a functional-flow unit might be approached to zero in a wide-scale network when N is huge. The prediction is more manageable and reliable in the macroscopic range when homogeneous mixing is assumed. Furthermore, it must be highlighted that the mathematical approach does not account for mortality (i.e., major road damage that would render them impassable once the floodwaters have subsided). While substantially damaged flood-damaged road cells are rare, It is rational and realistic to exclude the mortality. The model ingredient designed to reflect the temporal elements of flooding level utilizing macro attributes is built on the previous constructs (2).

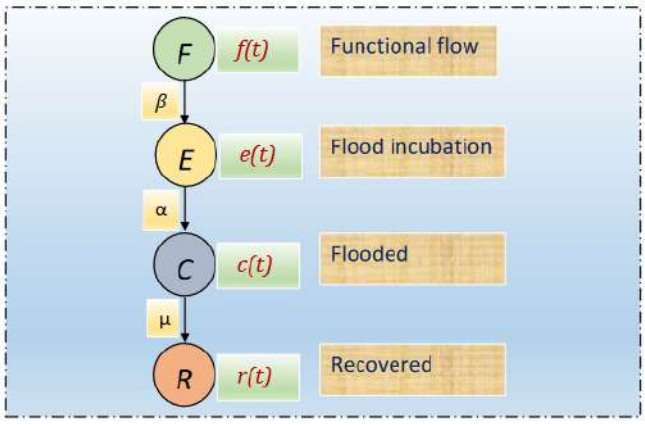

Figure 2. Flood spreading and recession in metropolitan roadway networks using a network percolation-based contagion model. The contagion model is used to calculate the flooding rate in cells.

4 Method of Solution

The approach and materials used in this work to forecast numerical solutions for the spread of floods on roads are described in this part.

4.1 Artificial Neural Networks

An acronym for a parallel architecture that is influenced by the way the central nervous system processes information is ANN. A series of interconnected computing devices known as a neural network gives computers A capability for learning and behavior similar to those of human brains. In conducting related studies, neuroscientists who study neurons in human and animal brains developed the idea of neural

networks. Artificial intelligence is a field that is constantly working to give computers the capacity to process data and draw results in a way that resembles humans. An artificial neural network, which is an area of artificial intelligence, is a cutting-edge concept in this field. Although there are various alternative ANN designs, the multi-layer feed-forward neural network, is the most widely used one. A mathematical description of an ANN's framework is as follows:

$$y_j = A_i(\sum_{j=1}^{n} w_j x_j + b_j), \tag{7}$$

here, x_j refers to the inputs, n for the amount of samples, w_j for weighing the connection, The bias vector is symbolized by b_j and activation function is symbolized by A_i. The weighted vectors w_1, w_2, w_3,...., w_n, weights and the n-dimensional input vectors x_1, x_2, x_3...., xn are used to parameterize the activation function $A(x, w)$. An S-shaped, curved sigmoid function serves as the activation function in this scenario (log sigmoid).

$$A_i = \frac{1}{1 + e^{-(wx+b)}}. \tag{8}$$

The feed-forward neural network (FNN), commonly referred to as the MLP is a type of neural network that has a hidden layer between the input and output layers. The term "hidden layer" refers to this layer. The amount of neurons utilized within the network is shown by the amount located below the hidden layer. A controller for ANN is shown in Figure (3).

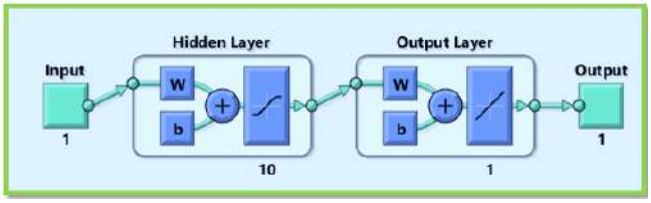

Figure 3. Artificial neural network controller.

4.2 ANN with LM Algorithm

Machine learning is the area of artificial intelligence that focuses on how to teach machines to learn from the information presented to them. Machine learning algorithms are a class of computing methods that "learn" data straight from it as opposed to depending on a model equation. Artificial intelligence employs these algorithms (AI). These algorithms are capable of dynamic performance gains as more data points become available for learning. Also, the operational states of the suggested approach (NN-BLMA) are addressed below and illustrated in Figure (4).

- A numeric algorithm, such as the RK method for supervised machine learning technique, produces the initial collection of data. In this step, the predictive model's effectiveness on real datasets is evaluated.
- Furthermore, the feed-forward design of an artificial neural network (FFNN) with 10 neurons in the hidden portion is created in MATLAB using the NFTOOL, as illustrated in Figure (3). The 1251-point dataset from the starting stage is provided to the FFNN as targeted data. The dataset is divided into

testing, validation, and training for the FFNN model, with weightings of 15%, 70%, and 15% respectively.

- In models of feed-forward neural networks (FFNN), the objective function is frequently the mean squared error (MSE). The MSE calculates the average discrepancy between the output that was expected and what was actually produced. In order to increase the model's accuracy, the goal is to decrease this error throughout training. The fitness function (E) are being expressed mathematically as:

$$E = \frac{1}{m}(\sum_{j=1}^{m} \hat{y}_j - y_j). \tag{9}$$

where the projected value of the target variable for the j^{th} sample in a dataset is denoted by the symbol y_j

- A non-linear least-squares function is reduced using an optimization technique known as the Levenberg-Marquardt algorithm. To control the trade-off between exploitation and exploration, it combines the method of gradient descent and Gauss-Newton methods and makes use of damped components. Equations in nonlinear systems are often solved using it in applications like curve fitting, training for artificial neural networks, and these others. It is a useful technique for determining the optimal weights related to Equation's anticipated solution (9). The weights are adjusted by this algorithm until the difference between the actual and expected solution is minimally possible.

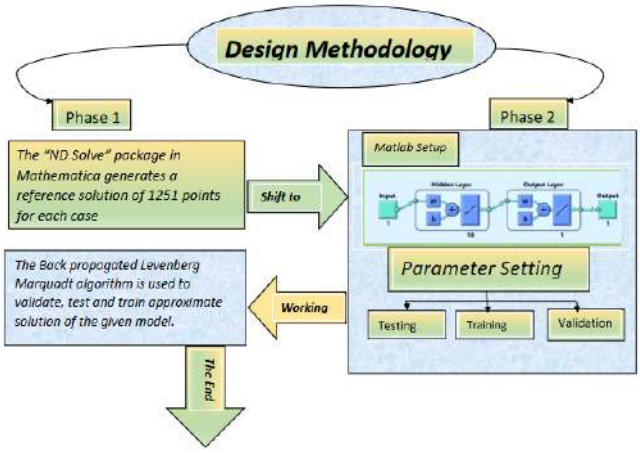

Figure 4. Flowchart of the design algorithm.

5 Results and Discussion

We analyze multiple instances of the mathematical model for flood spreading and recession in metropolitan roadway networks to assess the effectiveness and efficiency of the design methodologies. The variations in four factors—average degree k, rate of flood spreading β, rate of flood incubation α, and rate of recovery μ are used to determine the instances. We altered the parameter settings for each of the three scenarios. With a probability of 70% of test data, 15% of training data, and 15% of validation

data, the design technique yields outcome data sets. The mean squared error (MSE) of the design technique is displayed in the performance graph. The design technique illustrates the best validation performance in Figure (5), Figure (6), and Figure (7) because the error is minimized after a few training epochs, but the network may perform better on the validation data set if it starts to over-fit the training set. The scenario 1 outcomes for performance fall between 2.0468×10^{-10}, 1.2775×10^{-09}, 1.5932×10^{-10} and 1.5064×10^{-12}. Similar to instance 1, scenario 2 and scenario 3 performance data fall between 9.4136×10^{-11}, 1.7621×10^{-09}, 4.416×10^{-11}, 1.0663×10^{-11}, 2.2113×10^{-11}, 1.328×10^{-09}, 1.9832×10^{-10} and 1.2305×10^{-09} respectively.

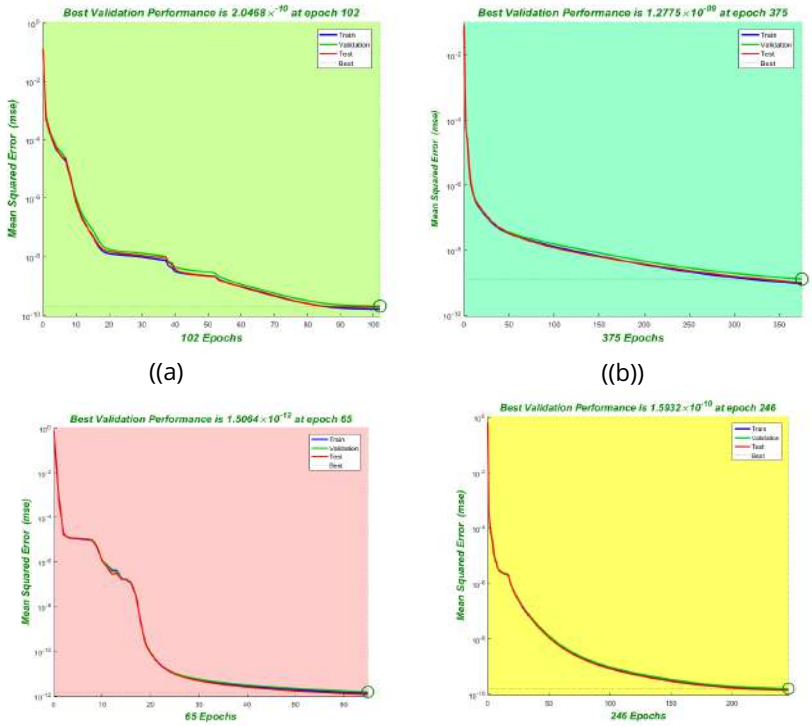

Figure 5. The mean square error of the NN-BLMA for the consequences of flood propagation and recession for scenario 1.

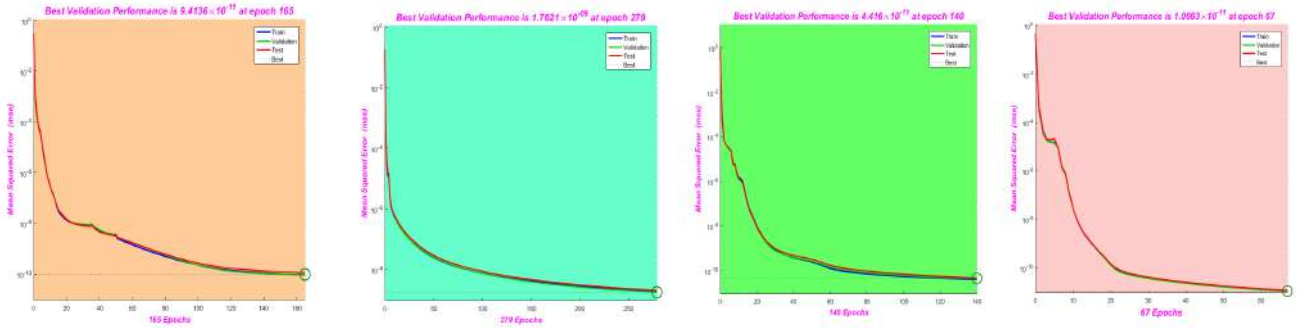

Figure 6. The mean square error of the NN-BLMA for the consequences of flood propagation and recession for scenario 2.

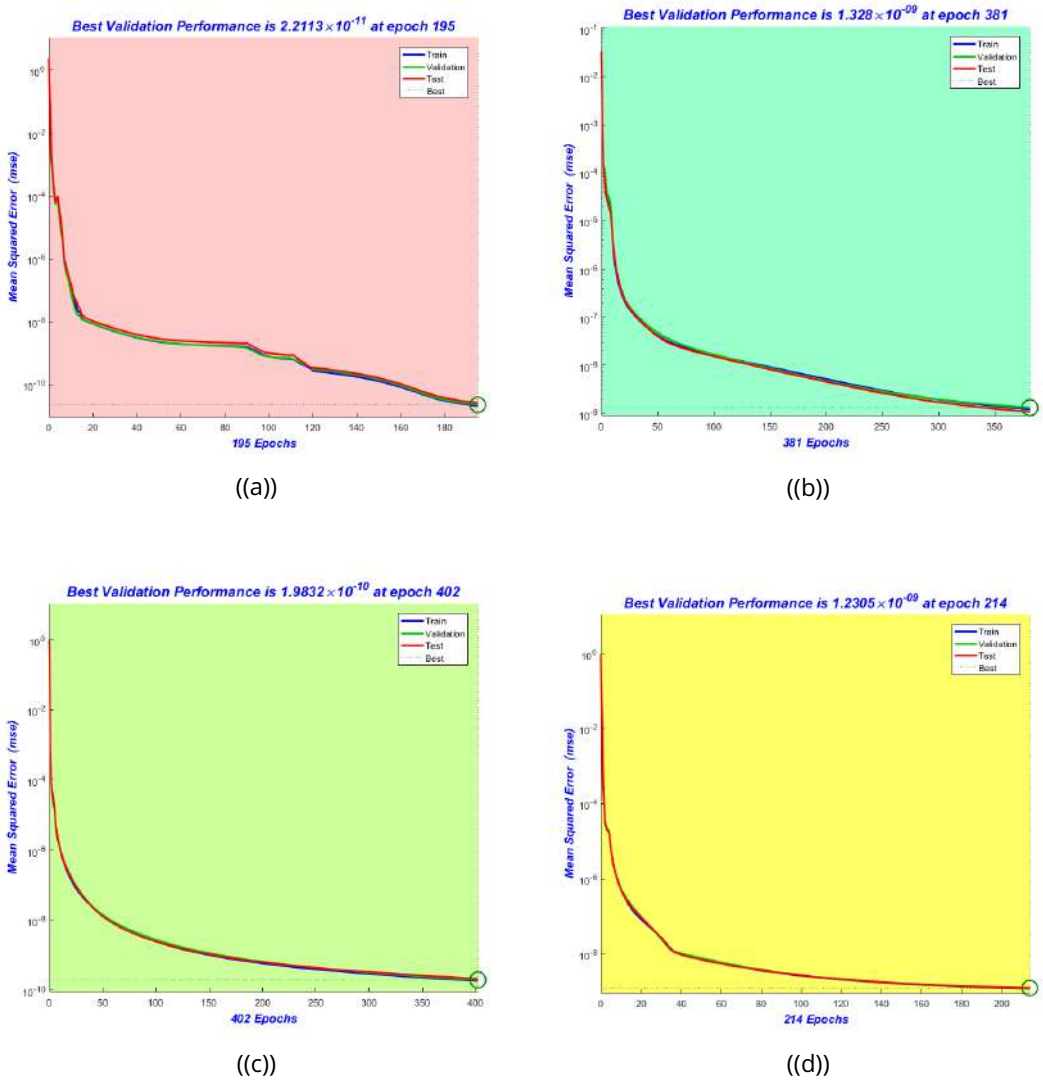

Figure 7. The mean square error of the NN-BLMA for the consequences of flood propagation and recession for scenario 3.

The statistical performance of each instance in regard to mu, gradient, and validation failures is displayed in Figure (8), (9), and (10). For case 1, the gradient values range around 9.5798×10^{-08}, 9.9573×10^{-08}, 9.8544×10^{-08} and 9.7364×10^{-08}, while the values for scenario 2 and 3 are 9.0153×10^{-08}, 9.9528×10^{-08}, 9.962×10^{-08}, 9.771×10^{-08}, 9.5629×10^{-08}, 9.8994×10^{-08},9.9463×10^{-08} and 9.8852×10^{-08} respectively. All cases' mu values fall within the range of 1×10^{-08} to 1×10^{-11}. The regression plot displays the network outcome in relation to the target for the sets of training, validation, and test. A perfect match requires that the data lie on a line with a 45-degree angle where the network outcomes and targets are equal. The regression figure shows us that R = 1 is the value when the data are at a 45-degree angle. Figures (11) of this article display the regression analysis for each scenario.

Regression values are 1 in all situations using equation (10), according to the figures, exactly matching the network and the targets.

$$R^2 = 1 - \frac{\sum_{j=1}^{m}(\hat{y}_j(t) - \bar{y}_j(t))^2}{\sum_{j=1}^{m}(y_j(t) - \bar{y}_j(t))^2)}, \tag{10}$$

$$AE = |x_j(t) - \hat{x}_j(t)|, \tag{11}$$

m is the amount of mesh points, while x_j, $\bar{x}_j$, and $\hat{x}_j$ stand for the reference, approximation, and mean of the solution at the jth input. The MSE and AE should both equal zero for perfect fitting, whereas R^2 should equal one.

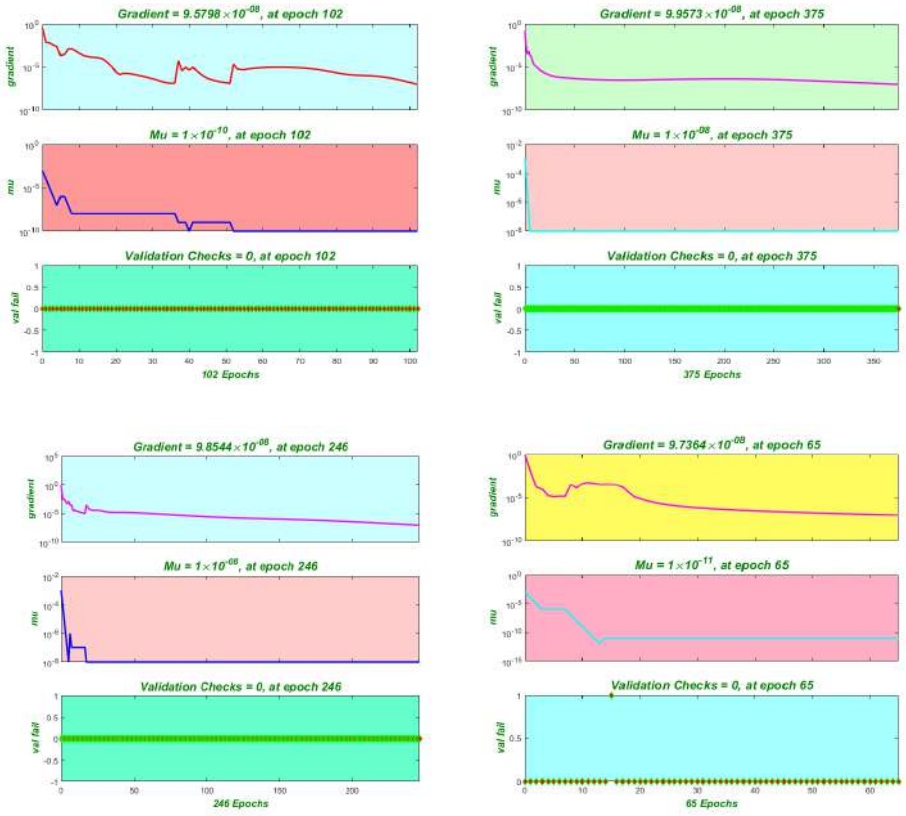

Figure 8. NN-BLMA Performance depending on gradient, mu, and validation failures throughout the optimization process for scenario 1.

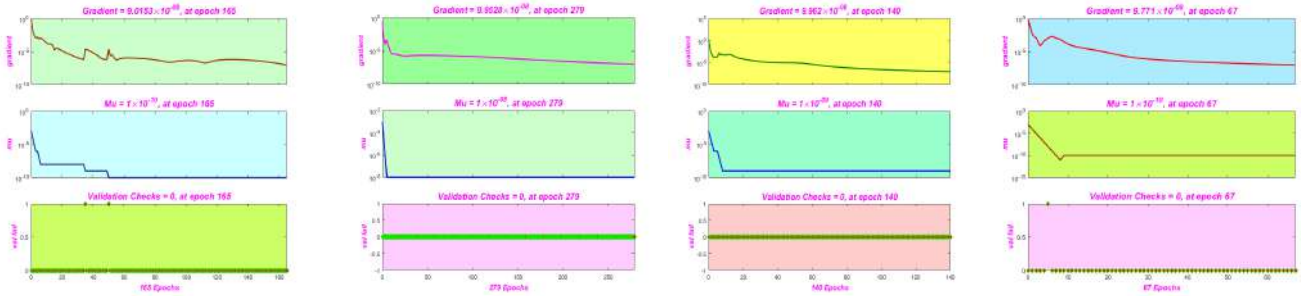

Figure 9. NN-BLMA Performance depending on gradient, mu, and validation failures throughout the optimization process for scenario 2.

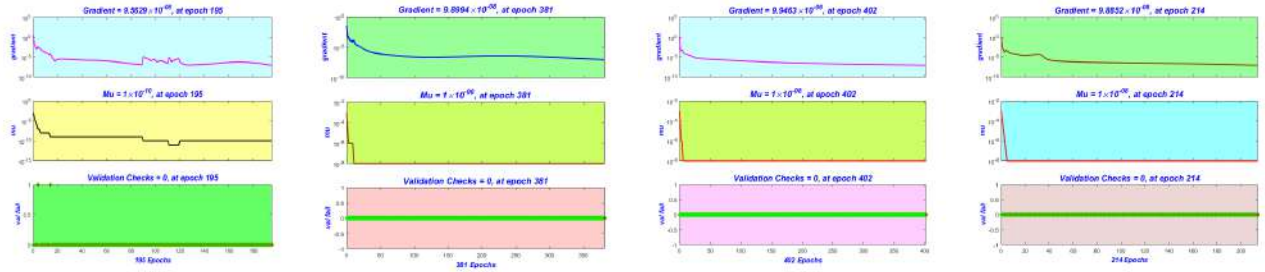

((a)) ((b)) ((c)) ((d))

Figure 10. NN-BLMA Performance depending on gradient, mu, and validation failures throughout the optimization process for scenario 3.

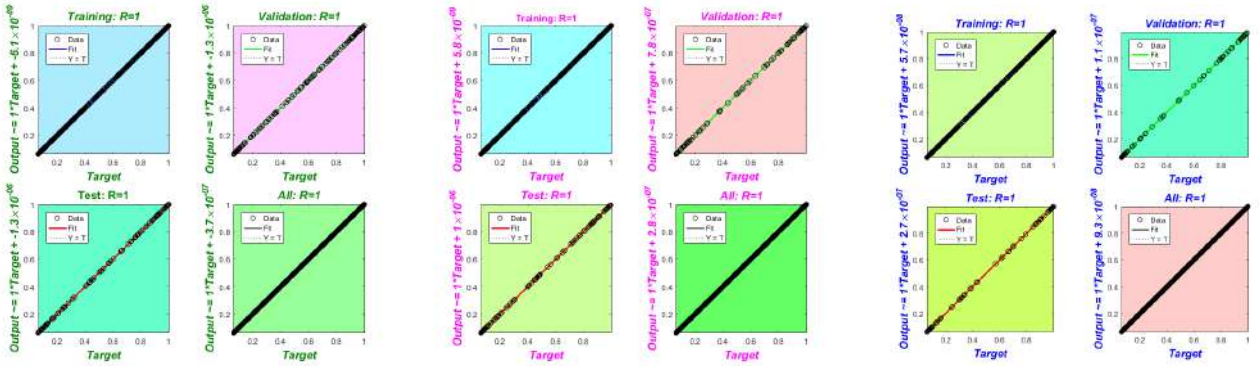

((a)) scenario 1 ((b)) scenario 2 ((c)) scenario 3

Figure 11. Analyzing the Role of α, β, μ, k in flood propagation Using Regression.

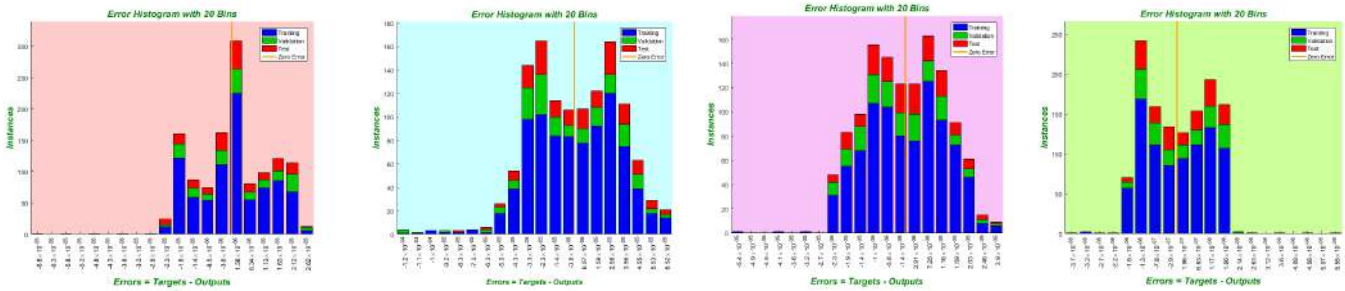

((a)) ((b)) ((c)) ((d))

Figure 12. Histogram study of the differences between the targeted data and approximative solution for scenario 1.

Figure (12), Figure (13), and Figure (14) display the histogram of errors among the targets and outputs during neural network training. Using distinct color bars, the errors within the training, validation, and testing data are highlighted. The majority of the points' error bars are quite close to the zero error line, indicating that the targets and the outputs are accurately matched and have the fewest faults. This demonstrates the precision of our design method. For instance 1, a flawed values fall between 10^{-05} to 10^{-06}, 10^{-04} to 10^{-06}, 10^{-05} to 10^{-06}, and 10^{-06} to 10^{-07}. For case 2 and case 3, the error values fall between 10^{-05} to 10^{-07}, 10^{-04} to 10^{-06}, 10^{-05} to 10^{-07}, 10^{-05} to 10^{-07}, 10^{-05} to 10^{-07}, 10^{-04} to 10^{-06}, 10^{-05} to 10^{-07}, and 10^{-04} to 10^{-06} respectively. Likewise, the fitness curves for different cases are illustrated in Figure (15), (16), and (17) respectively.

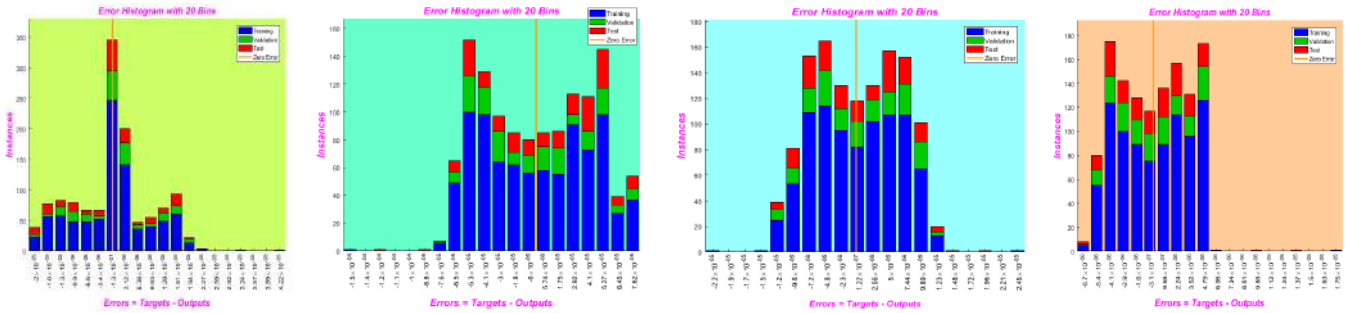

Figure 13. Histogram study of the differences between the targeted data and approximative solution for scenario 2.

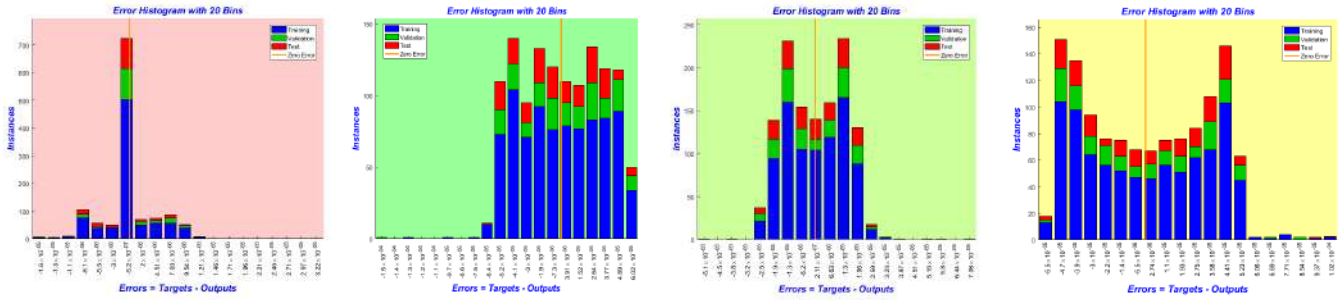

Figure 14. Histogram study of the differences between the targeted data and approximative solution for scenario 3.

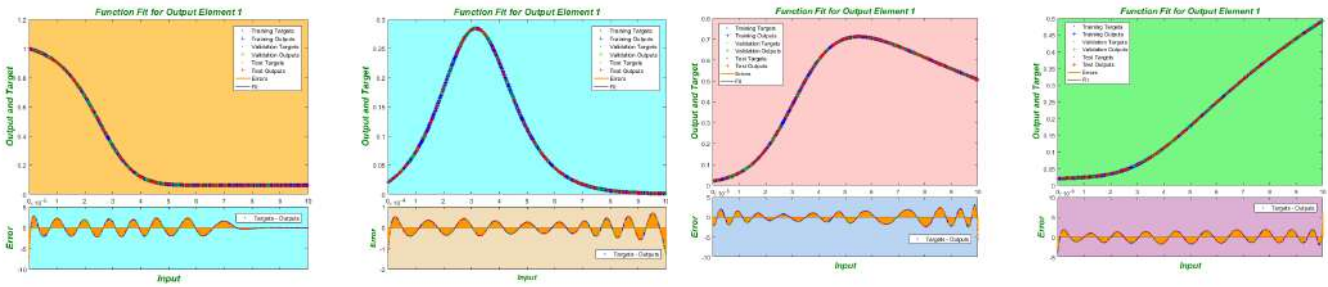

Figure 15. Performing a comparative analysis of the approximate solutions that were generated by NN-BLMA and the numerical solutions for scenario 1.

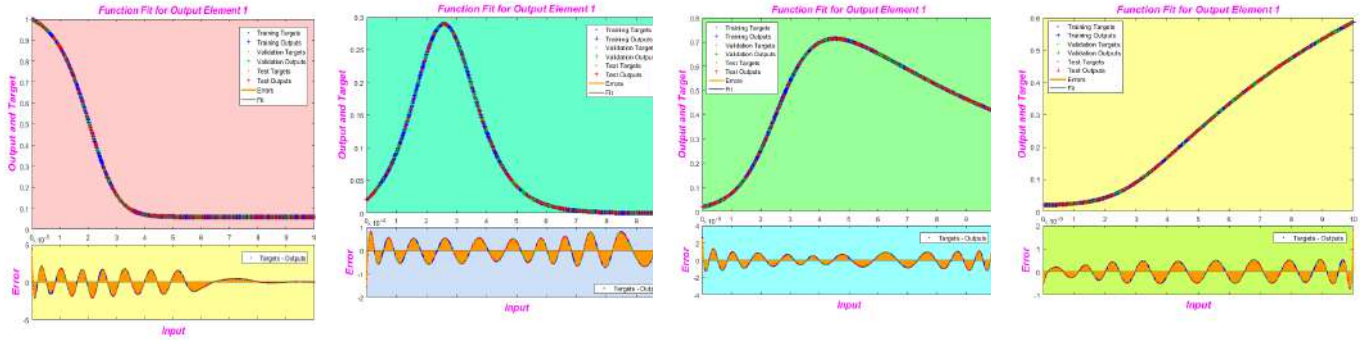

Figure 16. Performing a comparative analysis of the approximate solutions that were generated by NN-BLMA and the numerical solutions for scenario 2.

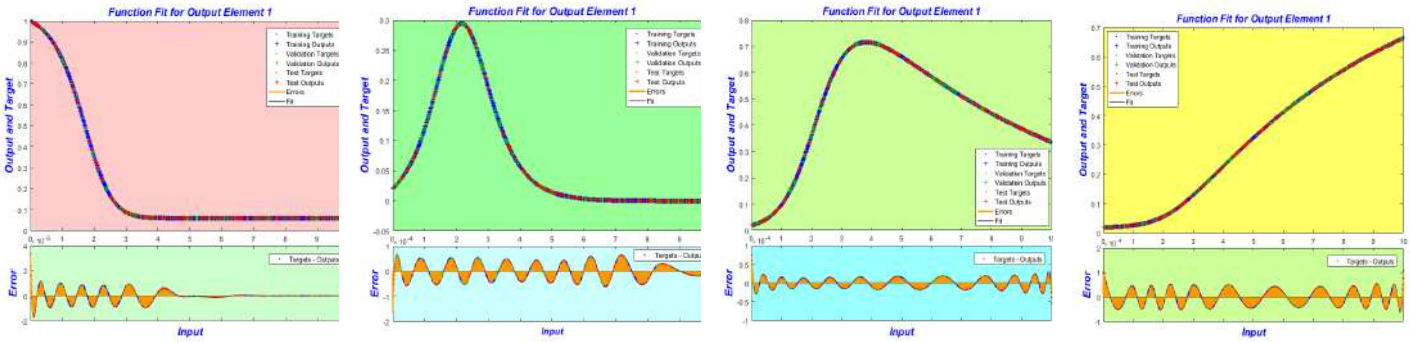

Figure 17. Performing a comparative analysis of the approximate solutions that were generated by NN-BLMA and the numerical solutions for scenario 3.

The data set offered by the computing system is demonstrated in the tables below. The effectiveness results in validation, training, testing, etc. are displayed in the tables. The best performance information for each of the three scenarios is shown in Table (1). The tables also include the amount of iterations, regression, and hidden neurons for each scenario.

Additionally, Figure (18) correlates the outputs (solution obtained by running NN-BLMA) to the targets (numerical solution of the paradigm) acquired via the "ND-Solve" package in Mathematica. The solid serves as the solution by NN-BLMA, while the cross lines display the result of numerically solving the model using Mathematica's "NDSolve" package. The accuracy of our design method is demonstrated by the fact that the solutions from NN-BLMA fall precisely on the targets' solution lines in the figure. When

Table 1. Statistical analysis of the values of the validation, testing, and training data along with performance measures computed for the error in the solutions of flood propagation.

Cases	*functions*	*Hidden Neurons*	*Training*	*Validation*	*Testing*	*Gradient*	*Mu*	*Epochs*	*Regression*
Case 1	*f(t)*	*10*	1.6×10^{-10}	2.1×10^{-10}	1.9×10^{-10}	9.95×10^{-08}	1×10^{-10}	*102*	*1*
	e(t)	*10*	9.3×10^{-10}	1.3×10^{-09}	1×10^{-09}	9.96×10^{-08}	1×10^{-08}	*375*	*1*
	c(t)	*10*	1.5×10^{-10}	1.6×10^{-10}	1.4×10^{-10}	9.85×10^{-08}	1×10^{-08}	*246*	*1*
	r(t)	*10*	1.3×10^{-12}	1.5×10^{-12}	1.2×10^{-12}	9.74×10^{-08}	1×10^{-11}	*65*	*1*
Case 2	*f(t)*	*10*	9.2×10^{-11}	9.4×10^{-11}	1.1×10^{-10}	9.0×10^{-08}	1×10^{-10}	*165*	*1*
	e(t)	*10*	1.8×10^{-09}	1.7×10^{-09}	2.02×10^{-09}	9.95×10^{-08}	1×10^{-08}	*279*	*1*
	c(t)	*10*	4.1×10^{-11}	4.4×10^{-11}	4.7×10^{-11}	9.96×10^{-08}	1×10^{-09}	*140*	*1*
	r(t)	*10*	1.1×10^{-11}	1.0×10^{-11}	1.1×10^{-11}	9.77×10^{-08}	1×10^{-10}	*67*	*1*
Case 3	*f(t)*	*10*	2.1×10^{-11}	2.2×10^{-11}	2.5×10^{-11}	9.56×10^{-08}	1×10^{-10}	*195*	*1*
	e(t)	*10*	1.2×10^{-09}	1.3×10^{-09}	1.1×10^{-09}	9.9×10^{-08}	1×10^{-08}	*381*	*1*
	c(t)	*10*	1.9×10^{-10}	2.0×10^{-10}	2.1×10^{-10}	9.95×10^{-08}	1×10^{-08}	*402*	*1*
	r(t)	*10*	1.21×10^{-09}	1.23×10^{-09}	1.2×10^{-09}	9.89×10^{-08}	1×10^{-08}	*214*	*1*

compared, The time it takes to get to the maximum point of flooding and the amount of flooded units at the maximum would both decline as the dispersion rate (β) and rate of flood incubation (α) increased. The amount of flooded units at the highest point is greatly reduced by a rise in rate of recovery μ, while the development rate of the flooded cells is increased by a rise in average degree k of the networks. The tables below provide an illustration of the comparison between the statistical data provided by the Mathematica 'NDSlove' package and the results of NN-BLMA. The contrasting examination of the two solutions for scenario 1 is presented in Table (2), while the scenario 2and scenario 3's comparisons can be seen in Table (4) and Table (6), accordingly, and their absolute differences are shown by Figure (19) and Tables (3), (5), (7) respectively.

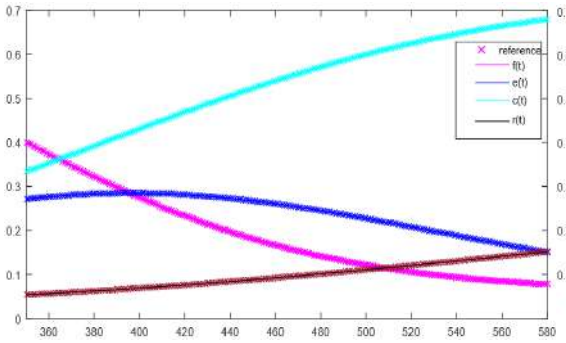

((a)) Comparison graph for case 1
α = 1,β = 1, μ = 0.1, k=3.

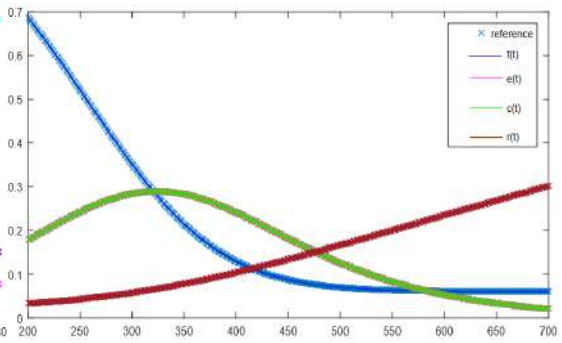

((b)) Comparison graph for case 2
α = 1.2, β = 1.2, μ = 0.12, k=3.1.

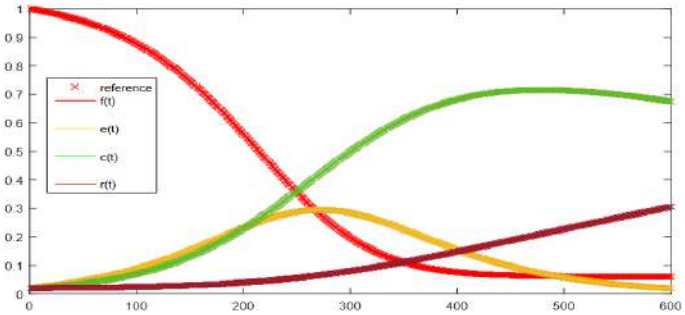

((c)) Comparison graph for case 3
α = 1.4, β = 1.4, μ = 0.14, k=3.2.

Figure 18. Comparison between RK-4 and NN-BLMA solutions of each case.

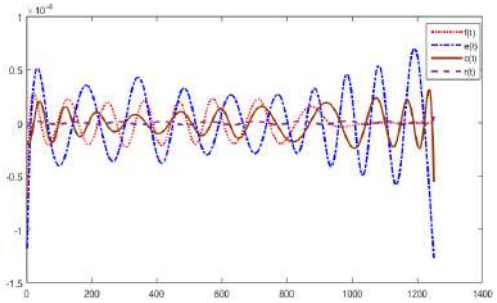

((a)) Absolute difference RK-4 and NN-BLMA for case 1
α = 1,β = 1, μ = 0.1, k=3.

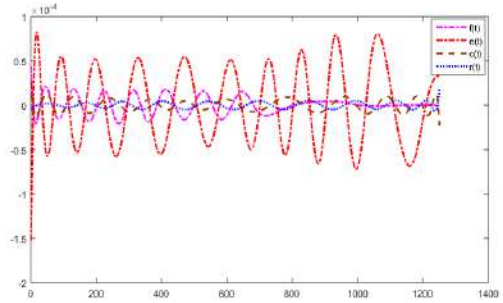

((b)) Absolute difference RK-4 and NN-BLMA for case 2
α = 1.2, β = 1.2, μ = 0.12, k=3.1.

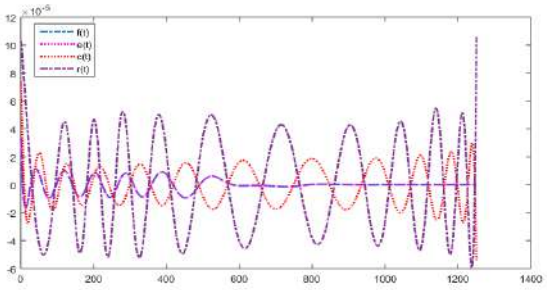

((c)) Absolute difference RK-4 and NN-BLMA for case 3
α = 1.4, β = 1.4, μ = 0.14, k=3.2.

Figure 19. Absolute difference RK-4 and NN-BLMA solutions of each case.

Table 2. Analysis of the numerical solution in comparison to the results of the NN-BLMA for case 1.

	f(t)		*e(t)*		*c(t)*		*r(t)*	
input	*RK-4*	*NN-BLMA*	*RK-4*	*NN-BLMA*	*RK-4*	*NN-BLMA*	*RK-4*	*NN-BLMA*
0	1	1.0001	0.02	0.02012	0.02	0.02002	0.02	0.02001
1	0.905	0.905	0.0725	0.073	0.0592	0.0592	0.0236	0.0236
2	0.674	0.673	0.182	0.182	0.170	0.171	0.034	0.0343
3	0.332	0.333	0.282	0.282	0.385	0.385	0.0613	0.062
4	0.121	0.121	0.226	0.227	0.601	0.602	0.112	0.112
5	0.068	0.068	0.112	0.112	0.702	0.702	0.177	0.178
6	0.061	0.061	0.045	0.0451	0.7054	0.7055	0.248	0.24853
7	0.0602	0.0602	0.017	0.0170	0.665	0.666	0.3172	0.3172
8	0.0601	0.0601	0.0063	0.0063	0.612	0.612	0.381	0.381
9	0.06001	0.06001	0.0023	0.0023	0.558	0.558	0.439	0.440
10	0.060	0.060	0.0009	0.0010	0.506	0.507	0.492	0.493

Table 3. Absolute difference between RK-4 and NN-BLMA.

Input	*Absolute difference in f(t)*	*Absolute difference in e(t)*	*Absolute difference in c(t)*	*Absolute difference in r(t)*
0	7.06×10^{-05}	1.18×10^{-04}	1.75×10^{-05}	3.94×10^{-06}
1	2.24×10^{-05}	2.22×10^{-05}	1.33×10^{-05}	4.51×10^{-08}
2	1.94×10^{-05}	3.10×10^{-05}	3.79×10^{-06}	5.34×10^{-08}
3	1.31×10^{-05}	7.61×10^{-06}	3.96×10^{-06}	5.01×10^{-07}
4	8.58×10^{-06}	2.31×10^{-05}	2.71×10^{-06}	1.54×10^{-06}
5	1.71×10^{-05}	2.64×10^{-05}	2.82×10^{-06}	1.73×10^{-06}
6	5.03×10^{-06}	1.57×10^{-05}	7.67×10^{-06}	9.05×10^{-07}
7	1.55×10^{-05}	2.79×10^{-05}	3.32×10^{-06}	5.21×10^{-07}
8	2.38×10^{-06}	2.07×10^{-05}	2.31×10^{-05}	1.25×10^{-06}
9	9.89×10^{-08}	5.02×10^{-05}	2.25×10^{-05}	7.94×10^{-07}
10	3.98×10^{-08}	1.27×10^{-04}	5.57×10^{-05}	5.80×10^{-06}

Table 4. Analysis of the numerical solution in comparison to the results of the NN-BLMA for case 2.

	f(t)		e(t)		c(t)		r(t)	
input	RK-4	NN-BLMA	RK-4	NN-BLMA	RK-4	NN-BLMA	RK-4	NN-BLMA
0	1	0.991	0.02	0.02025	0.02	0.019	0.02	0.0201
1	0.8661	0.8662	0.093	0.093	0.075	0.076	0.024	0.025
2	0.517	0.518	0.24	0.244	0.255	0.256	0.043	0.0432
3	0.1640	0.1641	0.265	0.265	0.53	0.540	0.090	0.0910
4	0.069	0.070	0.12	0.125	0.698	0.70	0.167	0.168
5	0.0606	0.0607	0.0417	0.0416	0.705	0.7051	0.252	0.2525
6	0.060	0.060	0.0129	0.0128	0.65	0.652	0.33	0.334
7	0.0600	0.0600	0.00391	0.0039	0.588	0.587	0.409	0.408
8	0.060	0.060	0.0012	0.0013	0.52	0.53	0.476	0.475
9	0.060	0.0601	0.0003	0.0004	0.46	0.47	0.54	0.53
10	0.060	0.0602	0.0001	7.38×10^{-05}	0.412	0.413	0.587	0.588

Table 5. Absolute difference between RK-4 and NN-BLMA.

Input	Absolute difference in f(t)	Absolute difference in e(t)	Absolute difference in c(t)	Absolute difference in r(t)
0	4.38×10^{-05}	1.53×10^{-04}	2.58×10^{-05}	5.39×10^{-06}
1	1.72×10^{-05}	3.26×10^{-05}	9.32×10^{-06}	2.05×10^{-06}
2	7.41×10^{-06}	5.18×10^{-05}	7.04×10^{-06}	9.03×10^{-08}
3	1.05×10^{-05}	3.28×10^{-05}	5.18×10^{-06}	1.22×10^{-06}
4	1.54×10^{-06}	1.59×10^{-05}	6.68×10^{-07}	1.69×10^{-06}
5	7.49×10^{-06}	3.99×10^{-05}	2.91×10^{-06}	4.76×10^{-06}
6	8.21×10^{-06}	8.15×10^{-06}	4.99×10^{-06}	2.79×10^{-06}
7	4.02×10^{-06}	6.44×10^{-05}	8.70×10^{-06}	2.55×10^{-06}
8	2.66×10^{-07}	6.95×10^{-05}	2.12×10^{-06}	4.76×10^{-06}
9	1.60×10^{-07}	3.27×10^{-05}	7.26×10^{-06}	4.79×10^{-06}
10	2.95×10^{-07}	3.29×10^{-05}	2.31×10^{-05}	1.82×10^{-05}

Table 6. Analysis of the numerical solution in comparison to the results of the NN-BLMA for case 3.

	f(t)		e(t)		c(t)		r(t)	
input	RK-4	NN-BLMA	RK-4	NN-BLMA	RK-4	NN-BLMA	RK-4	NN-BLMA
0	1	0.99	0.02	0.019	0.02	0.019	0.02	0.019
1	0.81	0.817	0.118	0.097	0.0973	0.0972	0.0268	0.0267
2	0.353	0.354	0.288	0.3621	0.3620	0.3621	0.0564	0.0565
3	0.0881	0.0880	0.1885	0.654	0.653	0.654	0.13	0.12
4	0.0613	0.0612	0.057	0.7142	0.7141	0.7142	0.228	0.227
5	0.060	0.0601	0.0145	0.661	0.661	0.660	0.324	0.3247
6	0.060	0.0601	0.0036	0.585	0.584	0.5846	0.412	0.411
7	0.060	0.060	0.0009	0.511	0.5106	0.5107	0.489	0.488
8	0.06	0.060	0.000212	0.4446	0.445	0.444	0.556	0.555
9	0.060	0.060	5.4×10^{-05}	0.38	0.387	0.386	0.614	0.613
10	0.06	0.059	1.3×10^{-05}	0.336	0.3361	0.3362	0.664	0.663

Table 7. Absolute difference between RK-4 and NN-BLMA.

Input	Absolute difference in f(t)	Absolute difference in e(t)	Absolute difference in c(t)	Absolute difference in r(t)
0	3.34×10^{-05}	1.59×10^{-04}	7.40×10^{-05}	1.03×10^{-04}
1	8.97×10^{-06}	3.76×10^{-05}	1.53×10^{-05}	4.18×10^{-05}
2	8.26×10^{-06}	1.86×10^{-05}	7.06×10^{-06}	3.06×10^{-05}
3	7.60×10^{-06}	3.32×10^{-05}	1.25×10^{-05}	4.96×10^{-05}
4	2.88×10^{-06}	3.86×10^{-05}	8.59×10^{-06}	3.52×10^{-05}
5	6.44×10^{-07}	4.46×10^{-05}	1.48×10^{-05}	4.29×10^{-05}
6	1.15×10^{-06}	2.41×10^{-06}	1.30×10^{-06}	1.87×10^{-05}
7	1.39×10^{-07}	3.42×10^{-05}	1.49×10^{-05}	2.13×10^{-05}
8	1.86×10^{-09}	3.49×10^{-05}	7.78×10^{-06}	2.44×10^{-05}
9	1.00×10^{-09}	1.71×10^{-06}	1.03×10^{-05}	3.09×10^{-05}
10	3.43×10^{-09}	2.38×10^{-05}	5.43×10^{-05}	1.06×10^{-04}

6 Conclusion

We investigated an anticipating model that integrates flood propagation characterization and network fissure processes to forecast the spreading and recession of floods in metropolitan roadway networks by creating and applying a novel supervised machine learning technique. A machine learning strategy, a kind of artificial intelligence (AI), updates the weights of a neural network model to forecast estimated solutions utilizing a set of precise, probabilistic, and advanced optimization techniques. The model is derived as an ODE system that includes four aspects: the flood incubation rate α, degree k of the networks on average, the recovery rate μ, and the flood propagation rate β, akin to the SEIR model. The increment in spreading rate β and rate of flood incubation α would decline the time for achieving the maximum of flooding and the amount of flooded cells at its highest point. The amount of flooded cells at the peak is greatly decreased by an increment in recovery rate μ, whereas at the time of the spreading stage, an increase in the average degree k of the networks significantly accelerates the rate of rising of flooded cells. The outcomes were also compared with the most recent analytical approaches described in the work. Comparing the outcomes calculated by using our suggested machine learning approach to the most cutting-edge techniques currently accessible, they are competitive. Additionally, the design algorithm's solidity and symmetry are confirmed by the visual and statistical methodologies. Additionally, a significant amount of graphical and tabular data that exhibit the best results for the mean squared error, regression analysis, and histogram, serve to highlight the design method's accuracy.

Author Contributions

Muhammad Fawad Kha: Writing- Original draft preparation, Methodology. **Fazl Ullah Fazal**: Software, Validation.**Awais Khan**: Visualization, Supervision, Reviewing, and Editing.**Muhammad Saad**: Conceptualization, Investigation, Data Curation.

Compliance with Ethical Standards

It is declare that all authors don't have any conflict of interest. It is also declare that this article does not contain any studies with human participants or animals performed by any of the authors. Furthermore, informed consent was obtained from all individual participants included in the study.

References

[1] A. A. Ganin, M. Kitsak, D. Marchese, J. M. Keisler, T. Seager, and I. Linkov, "Resilience and efficiency in transportation networks," *Science Advances*, vol. 3, no. 12, pp. e1701079, 2017.

[2] E. E. Koks, J. Rozenberg, C. Zorn, M. Tariverdi, M. Vousdoukas, S. A. Fraser, J. W. Hall, and S. Hallegatte, "A global multi-hazard risk analysis of road and railway infrastructure assets," *Nature Communications*, vol. 10, no. 1, pp. 2677, 2019.

[3] D. Paprotny, A. Sebastian, O. Morales-Nápoles, and S. N. Jonkman, "Trends in flood losses in Europe over the past 150 years," *Nature Communications*, vol. 9, no. 1, pp. 1985, 2018.

[4] W. Wang, S. Yang, H. E. Stanley, and J. Gao, "Local floods induce large-scale abrupt failures of road networks," *Nature Communications*, vol. 10, no. 1, pp. 2114, 2019.

[5] C. Fan, C. Zhang, A. Yahja, and A. Mostafavi, "Disaster City Digital Twin: A vision for integrating artificial and human intelligence for disaster management," *International Journal of Information Management*, vol. 56, pp. 102049, 2021.

[6] S. Lhomme, D. Serre, Y. Diab, and R. Laganier, "Analyzing resilience of urban networks: A preliminary step towards more flood resilient cities," *Natural Hazards and Earth System Sciences*, vol. 13, no. 2, pp. 221–230, 2013.

[7] J. A. Pulcinella, A. M. E. Winguth, D. J. Allen, and N. D. Gangadhar, "Analysis of flood vulnerability and transit availability with a changing climate in Harris County, Texas," *Transportation Research Record*, vol. 2673, no. 6, pp. 258–266, 2019.

[8] D. Serre, B. Barroca, M. Balsells, and V. Becue, "Contributing to urban resilience to floods with neighbourhood design: The case of Am Sandtorkai/Dalmannkai in Hamburg," *Journal of Flood Risk Management*, vol. 11, pp. S69–S83, 2018.

[9] L. Lu, X. Wang, Y. Ouyang, J. Roningen, N. Myers, and G. Calfas, "Vulnerability of interdependent urban infrastructure networks: Equilibrium after failure propagation and cascading impacts," *Computer-Aided Civil and Infrastructure Engineering*, vol. 33, no. 4, pp. 300–315, 2018.

[10] X. Guan and C. Chen, "General methodology for inferring failure-spreading dynamics in networks," *Proceedings of the National Academy of Sciences*, vol. 115, no. 35, pp. E8125–E8134, 2018.

[11] M. Mousa, X. Zhang, and C. Claudel, "Flash flood detection in urban cities using ultrasonic and infrared sensors," *IEEE Sensors Journal*, vol. 16, no. 19, pp. 7204–7216, 2016.

[12] E. Ramsey, Z. Lu, Y. Suzuoki, A. Rangoonwala, and D. Werle, "Monitoring duration and extent of storm-surge and flooding in western coastal Louisiana marshes with Envisat ASAR data," *IEEE Journal of Selected Topics in Applied Earth Observations and Remote Sensing*, vol. 4, no. 2, pp. 387–399, 2011.

[13] A. M. Youssef, B. Pradhan, and S. A. Sefry, "Flash flood susceptibility assessment in Jeddah city (Kingdom of Saudi Arabia) using bivariate and multivariate statistical models," *Environmental Earth Sciences*, vol. 75, no. 1, pp. 12, 2016.

[14] E. M. Douglas, R. M. Vogel, and C. N. Kroll, "Trends in floods and low flows in the United States: Impact of spatial correlation," *Journal of Hydrology*, vol. 240, no. 1-2, pp. 90–105, 2000.

[15] R. Merz and G. Blöschl, "Flood frequency regionalisation—spatial proximity vs. catchment attributes," *Journal of Hydrology*, vol. 302, no. 1-4, pp. 283–306, 2005.

[16] P. C. Nayak, K. P. Sudheer, D. M. Rangan, and K. S. Ramasastri, "Short-term flood forecasting with a neurofuzzy model," *Water Resources Research*, vol. 41, 2005.

[17] F. Hossain, N. Katiyar, Y. Hong, and A. Wolf, "The emerging role of satellite rainfall data in improving the hydro-political situation of flood monitoring in the under-developed regions of the world," *Natural Hazards*, vol. 43, pp. 199–210, 2007.

[18] A. Mosavi, P. Ozturk, and K.-W. Chau, "Flood prediction using machine learning models: Literature review," *Water*, vol. 10, no. 11, pp. 1536, 2018.

[19] C. Fan, F. Wu, and A. Mostafavi, "A hybrid machine learning pipeline for automated mapping of events and locations from social media in disasters," *IEEE Access*, vol. 8, pp. 10478–10490, 2020.

[20] C. Fan, Y. Jiang, and A. Mostafavi, "Emergent social cohesion for coping with community disruptions in disasters," *Journal of the Royal Society Interface*, vol. 17, no. 164, pp. 20190778, 2020.

[21] M. Saberi, H. Hamedmoghadam, M. Ashfaq, S. A. Hosseini, Z. Gu, S. Shafiei, D. J. Nair, V. Dixit, L. Gardner, S. T. Waller, *et al.*, "A simple contagion process describes spreading of traffic jams in urban networks," *Nature Communications*, vol. 11, no. 1, pp. 1616, 2020.

[22] A.-L. Barabási and M. Pósfai, "The Barabási-Albert model," *Network Science*, vol. 371, pp. 20120375, 2013.

[23] C. C. McCluskey, "Complete global stability for an SIR epidemic model with delay—distributed or discrete," *Nonlinear Analysis: Real World Applications*, vol. 11, no. 1, pp. 55–59, 2010.

[24] A.-L. Barabási, *Network Science*. Cambridge, UK: Cambridge University Press, 2016.

[25] J. Gao, S. V. Buldyrev, H. E. Stanley, and S. Havlin, "Networks formed from interdependent networks," *Nature Physics*, vol. 8, no. 1, pp. 40–48, 2012.

[26] F. Ball, D. Mollison, and G. Scalia-Tomba, "Epidemics with two levels of mixing," *The Annals of Applied Probability*, pp. 46–89, 1997.

[27] J. C. Miller, "Percolation and epidemics in random clustered networks," *Physical Review E*, vol. 80, no. 2, pp. 020901, 2009.